A Fast Spatial-Domain Method for the Suppression of Excitation-Induced Spurious Modes in SCN TLM

Stefan Lindenmeier, *Member, IEEE*, Bertram Isele, Robert Weigel, *Senior Member, IEEE*, and Peter Russer, *Fellow, IEEE*

***Abstract*—An efficient method for the suppression of excitation-induced spurious modes in the symmetrical condensed node (SCN) transmission-line matrix (TLM) method is presented for the general case of dielectric, anisotropic, or lossy media in planar structures. A special mapping of the field-excitation onto the wave amplitudes of the TLM algorithm completely prevents the emanation of the spurious modes. The application of the mapping in the k–ω space can be done for waveguides with low computational effort. The method is generalized for planar structures with high spatial frequencies of the field at the discontinuities. We use precomputed field templates at the entrance of the three-dimensional (3-D) structures. The mapping is mainly done in the space domain based on the quasi-TEM propagation of the guided waves to keep the computational effort low. Instead of the four-dimensional (4-D) k–ω transformation, only independent one-dimensional (1-D) transformations to the wave coefficient of the conductors direction and ω are necessary. In the case of propagation with low dispersion, the expenditure can be further reduced to 1-D transformations with respect to ω. The efficiency of the present method is demonstrated by investigation of a coplanar waveguide and a triplate waveguide.**

***Index Terms*—Excitation, spurious modes, TLM.**

I. Introduction

FOR THE modeling of electromagnetic fields in monolithic microwave integrated circuits (MMIC's), accurate simulation tools are required. The discrete space- and time-domain methods find growing interest as computational power became increasingly available. One of these methods is the transmission-line matrix (TLM) method in which the electromagnetic field is modeled by a mesh of interconnected transmission lines. We consider symmetrical condensed nodes (SCN's) introduced by Johns [1], which were generalized for lossy media by Nailor and Desai [2], and which became the most popular type of node (see Fig. 1). The electromagnetic-field components have to be mapped onto wave amplitudes a_i $(i = 1, 2, \cdots, 12)$ which are defined at the interconnecting ports and onto the wave amplitudes a_j $(j = 13, 14, \cdots, 18)$, which in turn are defined on stubs in the node center [1]. Due to anisotropic propagation characteristics, nonphysical spurious modes are also excited [3]–[5].

In this paper, a novel method for the suppression of excitation-induced *spurious modes* in a TLM mesh is presented. In general, the TLM method based on SCN's is applicable to the simulation of dielectric, anisotropic, and lossy media in planar structures. In [3], the propagation characteristics of the physical and nonphysical modes have been classified for the SCN with stubs. Based on an initial field distribution and the special propagation characteristics of waves in the TLM algorithm, the excitation of *spurious modes* can be eliminated by a special treatment in the $\boldsymbol{k}$–ω domain. A key component within this procedure is the adequate mapping between field components and wave amplitudes. For structures incorporating discontinuities causing high spatial frequencies in the field distribution, the mapping in the $\boldsymbol{k}$–ω domain may lead to a high computational effort. In this paper, an improvement of this method is given. After generating a physical-field distribution in templates [7], [8] at the entrance of the three-dimensional (3-D) structures, the excitation of spurious modes are efficiently rejected by a processing in the spatial domain. This is done with very low computational effort by using the quasi-TEM propagation behavior of the waves in the waveguides at the entrance of the 3-D structures. The computational effort is reduced to two independent transformations with respect to the longitudinal wavenumber k_z and ω. For weakly dispersive propagation, the computational effort can be reduced further to a single temporal transformation. While the mapping of the electromagnetic-field components onto the wave amplitudes at the stubs a_{13-18} can be performed according to [1], a new mapping for the wave amplitudes a_{1-12} at the interconnecting ports is necessary for a spurious mode-free excitation. Based on the scattering and propagation processes at the TLM nodes, an eigenvalue problem covers the coupling between the wave

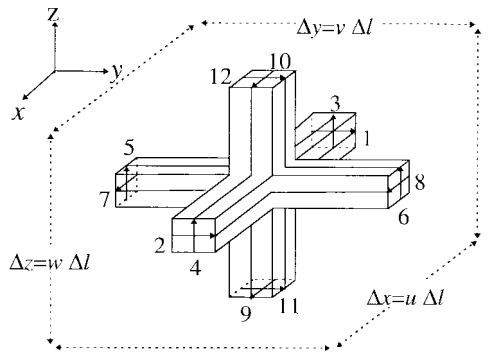

Fig. 1. Mesh cell of a 3-D symmetric-condensed TLM node with the mesh sizes Δx, Δy, Δz, and the arrows of the incident waves a_{1-12} of the connection lines (presentation without stubs).

Manuscript received October 8, 1996; revised July 18, 1997.

S. Lindenmeier, B. Isele, and P. Russer are with the Lehrstuhl für Hochfrequenztechnik, Technische Universität München, 80333 Munich, Germany.

R. Weigel was with the Lehrstuhl für Hochfrequenztechnik, Technische Universität München, 80333 Munich, Germany. He is now with the Technical University of Vienna, Vienna, Austria.

Publisher Item Identifier S 0018-9480(97)08015-0.

amplitudes a_{1-12} and the wave amplitudes a_{13-18} at the adjacent nodes. With that, the components of the wave-amplitude vector a_{1-12} can be determined recursively in an analytical way.

II. A Spurious Mode-Free Mapping of Field Quantities Onto Wave Amplitudes in $\boldsymbol{k}$–ω Space

The 18 incident waves at the node are combined in the vector $\boldsymbol{a}$ and the reflected waves in the vector $\boldsymbol{b}$. In the following, we consider the wave amplitudes in the $\boldsymbol{k}$–ω space:

$$\boldsymbol{a}(x,y,z,t), \boldsymbol{b}(x,y,z,t) \quad \circ\!\!-\!\!\bullet \; \boldsymbol{A}(k_x,k_y,k_z,\omega), \boldsymbol{B}(k_x,k_y,k_z,\omega). \tag{1}$$

The basic TLM algorithm can be written in the $\boldsymbol{k}$–ω domain as

$$T(\omega)\cdot \boldsymbol{B}(\boldsymbol{k},\omega) = [\boldsymbol{S}]_{18\times 18} \cdot \boldsymbol{A}(\boldsymbol{k},\omega) \tag{2}$$

$$\boldsymbol{A}(\boldsymbol{k},\omega) = [\boldsymbol{C}(\boldsymbol{k})]_{18\times 18}\cdot \boldsymbol{B}(\boldsymbol{k},\omega). \tag{3}$$

The time and space shift in (1) and (2) results in the time- and space-shift operators T, X, Y, Z, which can be combined in the matrix $\boldsymbol{C}(k)$. By eliminating the unknown wave-amplitude vector B and by the help of some additional basic matrix operations, an eigenvalue problem is established which separates the characteristics of the *physical modes* and the nonphysical *spurious modes*:

$$[\boldsymbol{K}]_{18\times 18}\cdot \boldsymbol{A} = \left(\begin{array}{c|c} [\boldsymbol{K_s}]_{12\times 12} & [\boldsymbol{K_q}]_{12\times 6} \\ \hline [\boldsymbol{O}]_{6\times 12} & [\boldsymbol{K_p}]_{6\times 6} \end{array}\right) \cdot \left(\begin{array}{c} \boldsymbol{A}_{1-12} \\ \hline \boldsymbol{A}_{13-18} \end{array}\right) = 0. \tag{4}$$

The trace matrix $\boldsymbol{K}_s$ relates to the propagation characteristics of the *spurious modes*. The condition $\det(\boldsymbol{K}_s)=0$ yields six eigenvalues according to the propagation characteristics of the six different spurious modes. These modes are propagating along the main axis of the TLM mesh with twice the speed of light, elucidating their nonphysical behavior. The propagation is accompanied by an alternation in sign at every time step. By solving the eigenvalue problem given in (4), a certain ratio of the wave amplitudes at the interconnecting ports to the wave amplitudes at the stubs is found, with which the excitation of spurious modes is prevented. With the submatrix $\boldsymbol{K}_q$, the coupling between the two sets of wave amplitudes A_{1-12} and A_{13-18} yields mapping rules, from which the wave amplitudes A_{1-12} are derived from the wave amplitudes at the stubs A_{13-18} without the excitation of spurious modes. The excitation and propagation characteristics of the spurious modes can be obtained from lines 1–12 of the system of equations (4). The condition $\det \boldsymbol{K}_s = 0$ leads to six double eigenvalues, which represent the propagation characteristics of six spurious modes. Considering the corresponding eigenvector solutions of $\boldsymbol{A}$ in (4), the following characteristics of the spurious modes can be derived:

- The six spurious modes are propagating in the different directions of $\pm\xi, (\xi = x,y,z)$ with the velocities $\Delta\xi/\Delta t$ and with a simultaneous oscillation in sign at every time step Δt.
- The excitation of a spurious mode, propagating in direction $\pm\xi$ is caused by superposition of two solutions of $\boldsymbol{A}$, which only consist of those two polarizations of wave amplitudes, which enter into the TLM nodes in direction $\pm\xi$.

The excitation and propagation characteristics of the physical modes modeling the electromagnetic phenomena, can be obtained from (4, rows 13–18). To relate the propagation characteristics of the physical modes to electromagnetic quantities, the mapping of the wave amplitudes A_{13-18} on the field components $E_x,\cdots,H_z$, which is introduced in [1], is done by the mapping matrix $\boldsymbol{Q}_C$ multiplied by the field vector $\boldsymbol{F}$:

$$\boldsymbol{A}_{13-18} = [\boldsymbol{Q}_C]_{6\times 6}\cdot \boldsymbol{F}. \tag{5}$$

With (5) and (4, rows 13–18), an eigenvalue problem can be formulated for the field vector $\boldsymbol{F}$ with the system matrix $\boldsymbol{M}$, which is

$$[\boldsymbol{M}]_{6\times 6} = [\boldsymbol{K}_p]_{6\times 6}\cdot[\boldsymbol{Q}_C]_{6\times 6}. \tag{6}$$

Therefore, the eigenvalue problem is given by

$$[\boldsymbol{M}]_{6\times 6}\cdot \boldsymbol{F} = \begin{pmatrix} \Omega_{\epsilon x} & 0 & 0 & 0 & K_z & -K_y \\ 0 & \Omega_{\epsilon y} & 0 & -K_z & 0 & K_x \\ 0 & 0 & \Omega_{\epsilon z} & K_y & -K_x & 0 \\ 0 & K_z & -K_y & \Omega_{\mu x} & 0 & 0 \\ -K_z & 0 & K_x & 0 & \Omega_{\mu y} & 0 \\ K_y & -K_y & 0 & 0 & 0 & \Omega_{\mu z} \end{pmatrix} \cdot \begin{pmatrix} E_x \\ E_y \\ E_z \\ H_x \\ H_y \\ H_z \end{pmatrix} = 0. \tag{7}$$

The system-matrix $\boldsymbol{M}$ includes the frequency-dependent coefficients $K_\xi, \Omega_{\epsilon\xi}, \Omega_{\mu\xi}, (\xi\eta,\zeta = x,y,z)$ as follows:

$$K_\xi = \frac{2}{\Delta\xi}\,\frac{\sin(k_\xi\Delta\xi)}{\cos(\omega\Delta t)+\cos(k_\xi\Delta\xi)} \tag{8}$$

$$\Omega_{\epsilon\xi} = W_\xi \epsilon_o\epsilon_{r\xi} - j\sigma_\xi \tag{9}$$

$$\Omega_{\mu\xi} = -W_\xi\mu_o\mu_{r\xi}, \qquad \text{with} \tag{10}$$

$$W_\xi = \left\{\frac{2}{\Delta t}\tan\left(\omega\frac{\Delta t}{2}\right)\right\}\left\{1+\frac{\Delta\xi\Delta l}{\Delta\eta\Delta\zeta h}\cdot\left[\frac{1-\cos(k_\eta\Delta\eta)}{\cos(\omega\Delta t)+\cos(k_\eta\Delta\eta)} + \frac{1-\cos(k_\zeta\Delta\zeta)}{\cos(\omega\Delta t)+\cos(k_\zeta\Delta\zeta)}\right]\right\}. \tag{11}$$

For very small mesh sizes $\Delta\xi/\lambda$ $(\xi = x,y,z)$, the coefficients $K_{x,y,z}$ approach their related propagation coefficients $k_{x,y,z}$, while the coefficients $W_{x,y,z}$ approach the frequency ω. Thus, (7) represents the TLM approach of Maxwell's curl-equations in the $\boldsymbol{k}$–ω space. The solution domain of the possible excitations of the physical modes is spanned by the eigenvectors $\boldsymbol{F}$ of (7). For small mesh sizes $\Delta\xi/\lambda$, this solution domain approaches the possible solutions due to Maxwell's equations. For large mesh sizes, the dispersive anisotropic character of the TLM-mesh dominates [10]. Thus, the solution domain by the eigenvectors of (7) sightly deviates from the solution domain containing the solutions to

Maxwell's equations. The implicit dispersion relation of the physical modes can be found by the requirement $\det \boldsymbol{M} = 0$ as

$$\begin{aligned}&\Omega_{\epsilon x}\Omega_{\epsilon y}\Omega_{\epsilon z}\Omega_{\mu x}\Omega_{\mu y}\Omega_{\mu z}\\&\quad+K_x^2\Omega_{\epsilon x}\Omega_{\mu x}(\Omega_{\epsilon y}\Omega_{\mu z}\Omega_{\epsilon z}\Omega_{\mu y})\\&\quad+K_y^2\Omega_{\epsilon y}\Omega_{\mu y}(\Omega_{\epsilon x}\Omega_{\mu z}+\Omega_{\epsilon z}\Omega_{\mu x})\\&\quad+K_z^2\Omega_{\epsilon z}\Omega_{\mu z}(\Omega_{\epsilon x}\Omega_{\mu y}+\Omega_{\epsilon y}\Omega_{\mu x})\\&\quad+(\Omega_{\epsilon x}K_x^2+\Omega_{\epsilon y}K_y^2+\Omega_{\epsilon z}K_z^2)\\&\quad\cdot(\Omega_{\mu x}K_x^2+\Omega_{\mu y}K_y^2+\Omega_{\mu z}K_z^2)=0.\end{aligned}\tag{12}$$

This equation can be solved explicitly for k_x, k_y, k_z, or ω in a few recursive steps for arbitrary anisotropic, lossy, dielectric media with arbitrary node-sizes u, v, w and a stability factor h. In case of free space, there exists only one solution for the frequency ω in the $\boldsymbol{k}$ space, while for the case of $\epsilon_r \neq \mu_r$ two solutions exist, which can be related to the two polarizations of electromagnetic waves in the medium. The two solutions overlap along the main axis and the space diagonals. In Fig. 2, solutions for both cases are presented in the $\boldsymbol{k}$ space.

While the mapping of the field components of the excitation on the wave-amplitudes A_{13-18} of the stubs can be done by (5), a new mapping of the field components on the wave amplitudes A_{1-12} at the cell boundary has to be developed out of (4) to prevent the excitation of the six spurious modes. The mapping is done by the mapping matrix $\boldsymbol{Q}_B$ of dimension 12×6:

$$\boldsymbol{A}_{1-12} = [\boldsymbol{Q}_B]_{12\times 6}\cdot\boldsymbol{F}.\tag{13}$$

Considering (4, rows 1–12), (5) and (13) lead to the new mapping matrix $\boldsymbol{Q}_B$:

$$[\boldsymbol{Q}_B]_{12\times 6} = -[\boldsymbol{K}_s]^{-1}_{12\times 12}\cdot[\boldsymbol{K}_q]_{12\times 6}\cdot[\boldsymbol{Q}_C]_{6\times 6}\tag{14}$$

with (15), shown at the bottom of the page, and

$$I_\zeta^{\pm} = \frac{\cos(\omega\Delta t/2)}{\cos(\omega\Delta t/2 \pm k_\zeta\Delta\zeta/2)}e^{\mp j(k_\zeta\Delta\zeta/2)},\qquad \zeta = x,y,z.\tag{16}$$

The elements of the mapping matrix $\boldsymbol{Q}_B$ are dependent on the space- and time-frequency. Thus, the field excitations have to be transformed into the $\boldsymbol{k}$–ω space before being mapped for the excitation of the wave amplitudes A_{1-18} to prevent the appearance of spurious portions of the excitation.

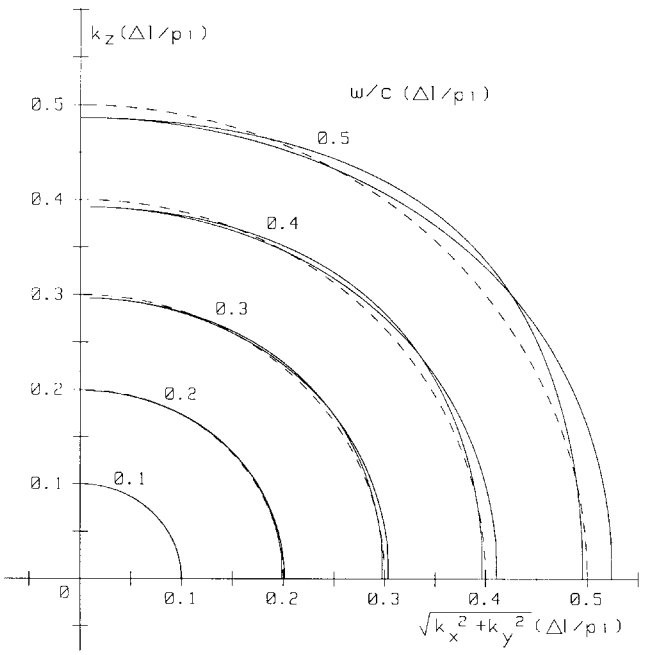

Fig. 2. Propagation characteristics of the physical modes in cross section $k_x = k_y$ in the $\boldsymbol{k}$ space. (Parameters of the mesh cells: $\varepsilon_r = 3$, $\mu_r = 1$, $\Delta x = \Delta y = \Delta z$, $h = 2$).

The mapping is verified by way of an example of the spectrum of the H_{101} mode in a rectangular cavity. Due to the fact that the dimensions of the resonator are multiples of the mesh-width $\Delta\zeta$ $(\zeta = x,y,z)$, spurious modes can resonate. The reduction of spurious modes by increasing the mesh density would lead to a high increase of computational effort. Fig. 3 shows the decrease of spurious portions of the resonance in a cavity with the number of cells in one length of the structure. The computational effort is determined by the number of matrix multiplications for the scattering at the TLM nodes. While the spurious modes decrease with an exponent of two, the computational effort increases by an exponent of four because of the linear increase of cells in every x-, y-, and z-directions, and the increase of the required time steps.

In contrast, the computational effort for the application of the mapping by matrix $\boldsymbol{Q}_B$ is low because of the few

$$[\boldsymbol{Q}_B]_{12\times 6} = \frac{1}{2\sqrt{Z_0}}\begin{pmatrix}0 & I_x^+v & 0 & 0 & 0 & I_x^+wZ_0\\0 & I_x^-v & 0 & 0 & 0 & -I_x^-wZ_0\\0 & 0 & I_x^+w & 0 & -I_x^+vZ_0 & 0\\0 & 0 & I_x^-w & 0 & I_x^-vZ_0 & 0\\0 & 0 & I_y^+w & I_y^+uZ_0 & 0 & 0\\0 & 0 & I_y^-w & -I_y^-uZ_0 & 0 & 0\\I_y^+u & 0 & 0 & 0 & 0 & -I_y^+wZ_0\\I_y^-u & 0 & 0 & 0 & 0 & I_y^-wZ_0\\I_z^+u & 0 & 0 & 0 & I_z^+vZ_0 & 0\\I_z^-u & 0 & 0 & 0 & -I_z^-vZ_0 & 0\\0 & I_z^+v & 0 & -I_z^+uZ_0 & 0 & 0\\0 & I_z^-v & 0 & I_z^-uZ_0 & 0 & 0\end{pmatrix}\tag{15}$$

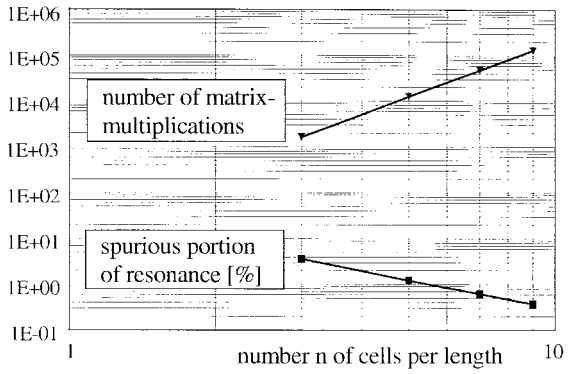

Fig. 3. Computation effort for reduction of spurious modes by increasing the resolution. (Numerical solution of spurious portions in the resonance of a cavity generated by conventional excitation for different cell numbers n in one row of the mesh.)

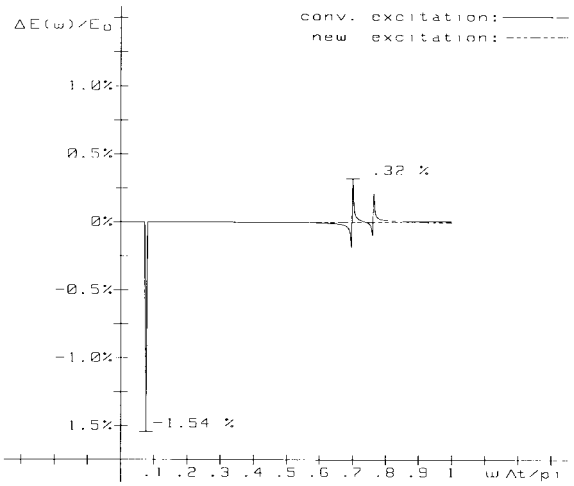

Fig. 4. Deviation of the resonance spectrum of a TLM simulation from the analytical spectrum of a rectangular cavity with cell parameters $\varepsilon_r = \mu_r = 1$, $\Delta x = \Delta y = \Delta z/2$, $h = 5$.

spatial frequencies in the field distribution of such a waveguide structure. In Fig. 4, the deviations between the calculated and the analytical spectrum of the E_y components are shown for the different excitation methods. Using a conventional excitation for the simulations, the occurrence of spurious modes is visible, whereas the excitation by matrix $\boldsymbol{Q}_B$ exhibits no spurious modes. Fig. 4 points out that the energy at the expected resonance frequency is decreased by the amount of energy stored in the spurious modes at high frequencies. These spurious effects are caused by a partial-mode conversion from physical modes to spurious modes and cannot be removed by low-pass filtering. The two different resonances for spurious modes occur due to the different cell sizes dependent on the x- and z-direction.

III. A Spatial-Domain Method for the Supression of Excitation-Induced Spurious Modes

A *spurious-mode-free* excitation template representing all wave amplitudes a_{1-18} at a plane perpendicular to the wave propagation is required for the accurate modeling of planar structures. The simulations of those structures yield field

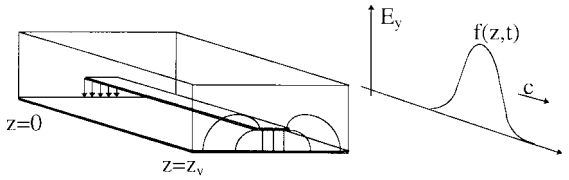

Fig. 5. Waveguide section with fine discretization for the computation of the preliminary field distribution. Nonphysical temporal Gaussian excitation at position $z = 0$, improved field distribution at $z = z_v$.

singularities with very high spatial frequencies. In that case, the mapping in the $\boldsymbol{k}$–ω space with a high number of frequencies would lead to a high computational effort. Thus, the mapping has to be performed in the space domain based on the quasi-TEM propagation of the guided waves in the entrance of the 3-D structures to keep the computational effort low. Instead of the four-dimensional (4-D) $\boldsymbol{k}$–ω transformation only two independent one-dimensional (1-D) transformations are necessary with respect to ω and the wave coefficient k_z of the conductors direction. As an example, we consider waveguide structures with the propagation in z-direction and excitation templates that are distributed in a plane perpendicular to the direction of propagation. As is depicted in [3], the *spurious modes* are caused by portions of the amplitudes a_{1-12}, which do not fulfill the physical relation between the interconnected wave amplitudes a_{1-12} and the amplitudes at the stubs a_{13-18}.

In a preprocessing step, we apply a fine discretization to a test section with the same cross section as the input section of the structure under investigation. This test section is excited in a conventional way. After the distance $z = z_v$, a field template is extracted for further processing. The propagation velocity c in the actual waveguide is also measured. Passing the test section, the field evolves itself and approaches the physical-field distribution (Fig. 5). A snapshot of the transversal-field distribution is extracted for the use as field template when the maximum of the incident pulse passes the chosen position $z = z_v$. In a first step, a conventional mapping is applied to the wave amplitudes at the stubs $a_{13-18}(x, y)$. The template consists of nodes. Due to the dispersion relation, which admits propagating modes at $k_x \Delta x = \pi$, $k\Delta y = \pi$ in the $\boldsymbol{k}$ space, additional *spurious modes* occur with a spatially alternating sign. However, if a sufficiently fine discretization and local low-pass filtering is applied, their influence can be minimized. This results in a nearly *spurious-mode-free* field template.

For the excitation of a field in a waveguide which propagates only in z-direction, it is sensible to excite the field along a cross section of the waveguide between the centers of the nodes, where only the waves a_{9-12} are defined. The excitation is done afterwards by only exciting the waves a_9 and a_{11}, which are propagating in the same direction. For these waves, a spurious-mode-free mapping of the exciting field is derived. The waves a_{9-12} are defined in the direction $\pm z$ of the waveguide (Fig. 1). The generation of those wave amplitudes from the amplitudes at the stubs a_{13-18} is based on the mapping in the $\boldsymbol{k}$–ω domain, as shown by (15). For example, the amplitude a_9 is given with respect to the transverse

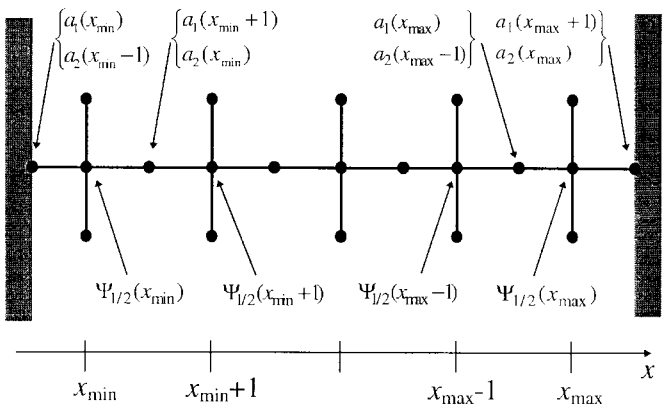

Fig. 6. Position of the variables within one line of nodes enclosed by boundary conditions in x-direction.

coordinates x and y by

$$A_9(x,y,k_z,\omega) = \frac{(1+T)}{(1+TZ)} \cdot \left(A_{13}(x,y,k_z,\omega) + \frac{A_{17}(x,y,k_z,\omega)}{Z_y} \right) = \frac{(1+T)}{(1+TZ)} \underline{\Psi}_9(x,y,k_z,\omega). \quad (17)$$

The function $\psi(x,y,z,t)$ representing the stub amplitudes, contains an amplitude function $\Psi(x,y)$ which is only dependent on the transversal coordinates

$$\Psi_9(x,y,z,t) = \left(a_{13}(x,y) + \frac{a_{17}(x,y)}{Z_y} \right) f(z,t) = \Psi_9(x,y) f(z,t). \quad (18)$$

Due to the fact that $f(z,t)$ describes the propagation of a pulse in z-direction with the constant velocity c, all dependencies from ω and k_z are combined in the function $\underline{\phi}_z(k_z,\omega)$. With (18) this leads to the function $\phi_z(z,t)$ as follows:

$$\Phi_{z9}(z,t) \overset{t}{\circ\!\!-\!\!\bullet} \underline{\phi}_{z9}(z,\omega) = \frac{1+e^{j\omega\Delta t}}{1+e^{j\omega(\Delta t+\Delta z/c)}} \underline{f}(z=0,\omega) e^{-j\omega z/c}. \quad (19)$$

Therefore, we have to perform only one single Fourier transform for each temporal excitation function. Afterwards we apply the function $\phi_z(z,t)$ for obtaining the amplitudes a_9 in the cross section under consideration:

$$a_9(x,y,z,t) = \Psi_9(x,y)\Phi_{z9}(z,t). \quad (20)$$

The waves a_{10-12} can be developed in an analogous way, corresponding to the new mapping in (15). If the excitation should be done in a cross section of the waveguide going through the centers of the nodes, the waves a_{1-8} have to be derived for the spurious-mode-free excitation. These waves are defined in the template perpendicular to the direction of the waveguide (Fig. 1). For their generation, rows of nodes within the template are considered. The templates have to be terminated in transverse direction by appropriate boundary conditions. The waves along one line of nodes are coupled with each other according to the boundary conditions at the transverse boundaries of the template. For the amplitudes a_{1-4}, we have to consider rows in x-direction, and for a_{5-8}, we have to consider rows in y-direction. The wave amplitudes are evolved in pairs $a_1-a_2, a_3-a_4, \cdots$, etc. Now we consider a row in x-direction, which is bounded by walls with fixed-boundary conditions. The position of the variables is shown in Fig. 6. The number $n_{x\max}$ of nodes in x-direction is given by the node numbers of the first and the last node of the following row:

$$n_{x\max} = x_{\max} - x_{\min} + 1. \quad (21)$$

The following relations in the $\boldsymbol{k}$–ω domain can be found for the amplitudes a_1 and a_2:

$$A_{1,2} = \frac{(1+T)}{(1+TX^{\pm 1})} (A_{14} \pm A_{18}/Z_z) \Rightarrow (X^{\pm 1})A_{1,2} = (1+1/T)(A_{14} \pm A_{18}/Z_z) - (1/T)A_{1,2}. \quad (22)$$

This can be expressed in the space domain as

$$\underline{a}_{1,2}(x \pm 1,y,z,\omega) = (1+1/T)(\underline{a}_{14}(x,y,z,\omega) \pm \underline{a}_{18}(x,y,z,\omega)/Z_z) - (1/T)\underline{a}_{1,2}(x,y,z,\omega) \quad (23)$$

and abbreviated with the functions $\underline{\Psi}$:

$$\underline{a}_1(x+1,y,z,\omega) = \underline{\Psi}_1(x,y,z,\omega) - (1/T)\underline{a}_1(x,y,z,\omega) \quad (24a)$$

$$\underline{a}_2(x-1,y,z,\omega) = \underline{\Psi}_2(x,y,z,\omega) - (1/T)\underline{a}_2(x,y,z,\omega). \quad (24b)$$

In the following, we consider the dependencies with respect to x and t. From (24a) and (24b), a relation between all a_1 and a_2 at a row with $n = 0,1,2,\cdots,n_{\max}$ and the corresponding starting values $a_1(x_{\min})$ and $a_2(x_{\max})$ at the boundary can be found:

$$\underline{a}_1(x_{\min}+(n+1),\omega) = \sum_{\nu=0}^{n} (-1/T)^{\nu} \underline{\Psi}_1(x_{\min}+n-\nu,\omega) + (-1/T)^{(n+1)} \underline{a}_1(x_{\min},\omega) \quad (25a)$$

$$\underline{a}_2(x_{\max}-(n+1),\omega) = \sum_{\nu=0}^{n} (-1/T)^{\nu} \underline{\Psi}_2(x_{\max}-n-\nu,\omega) + (-1/T)^{(n+1)} \underline{a}_2(x_{\max},\omega). \quad (25b)$$

This yields a relationship for the starting and end values at each row:

$$\underline{a}_1(x_{\max}+1,y,\omega) = \sum_{\nu=0}^{n_{x_{\max}}} (-1/T)^{\nu} \underline{\Psi}_1(x_{\max}-\nu,y,\omega) - (-1/T)^{(n_{\max}+1)} \underline{a}_1(x_{\min},y,\omega) \quad (26a)$$

$$\underline{a}_2(x_{\min}-1),y,\omega) = \sum_{\nu=0}^{n_{x_{\max}}} (-1/T)^{\nu} \underline{\Psi}_2(x_{\min}+\nu,y,\omega) - (-1/T)^{(n_{x_{\max}}+1)} \underline{a}_2(x_{\max},y,\omega). \quad (26b)$$

All rows of nodes are terminated at the enclosing boundaries by certain reflections coefficients. We choose either $w=-1$ corresponding to electrical walls and $w=1$ corresponding to magnetic walls, and found the relation between a_1 and a_2 at the boundaries as

$$\underline{a}_1(x_{\max}+1,\omega)=w_{x\,\max}\underline{a}_2(x_{\max},\omega) \tag{27a}$$

$$\underline{a}_2(x_{\min}-1,\omega)=w_{x\,\min}\underline{a}_1(x_{\min},\omega). \tag{27b}$$

From (26a) and (26b) and (27a) and (27b), we obtain the following system of equations:

$$\begin{aligned}&(-1/T)^{(n_{x\max}+1)}\,\underline{a}_1(x_{\min},\omega)+w_{\max}\underline{a}_2(x_{\max},\omega)\\&\quad=\sum_{\nu=0}^{n_{\max}}(-1/T)^{\nu}\underline{\Psi}_1(x_{\max}-\nu,\omega)\end{aligned} \tag{28a}$$

$$\begin{aligned}&w_{\min}\underline{a}_1(x_{\min},\omega)+(-1/T)^{(n_{x\max}+1)}\,\underline{a}_2(x_{\max},\omega)\\&\quad=\sum_{\nu=0}^{n_{x\max}}(-1/T)^{\nu}\underline{\Psi}_2(x_{\min}+\nu,\omega).\end{aligned} \tag{28b}$$

Also in the case of a quasi-TEM propagation of the pulse, the amplitudes at the stubs a_{14} and a_{18} may be separated into a time function $f(z,t)$ (here $f(t)$) and an amplitude function $a(x,y)$ (here $a(x)$). According to (18), we introduce function $\Psi(x)$, which is generally dependent on the transversal position $x,\ y$:

$$\begin{aligned}a_{14/18}(x,t)=a_{14/18}(x)f(t);\quad \underline{a}_{14/18}(x,\omega)=a_{14/18}(x)\underline{f}(\omega)\\ \Rightarrow\quad \underline{\Psi}_{1/2}(x,\omega)=\Psi_{1/2}(x)\underline{f}(\omega)(1+1/T).\end{aligned} \tag{29}$$

The functions $\Psi(x)$ are calculated in the time and space domain from the amplitudes at the following stubs:

$$\Psi_{1/2}(x,t)=\left(a_{14}(x,t)\pm\frac{a_{18}(x,t)}{Z_y}\right). \tag{30}$$

Therefore, we can write the functions with separate space and frequency dependencies as follows:

$$\begin{aligned}\underline{a}_1(x_{\min},\omega)=\sum_{\nu=0}^{n_{x\max}}\Bigg[&\Psi_1(x_{\max}-\nu)\\&\cdot\frac{(-T)^{-(n_{x\max}+\nu)}\underline{f}(\omega)(1+1/T)}{T^{-2n_{x\max}}-w_{\max}w_{\min}}\\&-\Psi_2(x_{\min}+\nu)\\&\cdot\frac{w_{\max}(-T)^{-\nu}(\underline{f}(\omega)(1+1/T)}{T^{-2n_{x\max}}-w_{\max}w_{\min}}\Bigg]\end{aligned} \tag{31a}$$

$$\begin{aligned}\underline{a}_2(x_{\max},\omega)=\sum_{\nu=0}^{n_{x\max}}\Bigg[&\Psi_2(x_{\min}+\nu)\\&\cdot\frac{(-T)^{-(n_{x\max}+\nu)}\underline{f}(\omega)(1+1/T)}{T^{-2n_{x\max}}-w_{\max}w_{\min}}\\&-\Psi_1(x_{\max}-\nu)\\&\cdot\frac{w_{\min}(-T)^{-\nu}(\underline{f}(\omega)(1+1/T)}{T^{-2n_{x\max}}-w_{\max}w_{\min}}\Bigg].\end{aligned} \tag{31b}$$

The impulse function $f(t)$ is transformed to the frequency domain, expanded to the function $\phi(\omega)$, and transformed back to the time domain as follows:

$$\Phi_x(t)\circ\!\!-\!\!\bullet\,\underline{\Phi}_x(\omega)=\frac{\underline{f}(\omega)(1+1/T)}{e^{-2jn_{x\max}\omega\Delta t}-w_{x\,\max}w_{x\,\min}}. \tag{32}$$

Due to the fact that this has to be done for only one transversal setup, the computational effort is kept considerably low. After the determination of the function $\phi(t)$, the boundary values $a_1(x_{\min},t)$, and $a_2(x_{\max},t)$ in (31a) and (31b) are given by

$$\begin{aligned}&a_1(x_{\min},t)\\&\quad=\sum_{\nu=0}^{n_{x\,\max}-1}(-1)^{\nu}\Big[\Psi_1(x_{\max}-\nu)(-1)^{n_{x\max}}\\&\qquad\cdot\Phi_x(t-\nu-n_{x\,\max})\\&\qquad-\Psi_2(x_{\min}+\nu)w_{x\,\max}\Phi_x(t-\nu)\Big]\end{aligned} \tag{33a}$$

$$\begin{aligned}&a_2(x_{\max},t)\\&\quad=\sum_{\nu=0}^{n_{x\,\max}-1}(-1)^{\nu}\Big[\Psi_2(x_{\min}+\nu)(-1)^{n_{x\max}}\\&\qquad\cdot\Phi_x(t-\nu-n_{x\,\max})\\&\qquad-\Psi_1(x_{\max}-\nu)w_{x\,\min}\Phi_x(t-\nu)\Big].\end{aligned} \tag{33b}$$

The amplitudes a_1 and a_2 on the row are calculated from starting values at $x_{\min}$ and $x_{\max}$, also in time and space domain:

$$\begin{aligned}a_1(x,t)=&\sum_{\nu=0}^{(x-x_{\min}-1)}\Big[(-1)^{\nu}\Psi_1(x-1-\nu)\Phi_x(t-\nu)\Big]\\&-(-1)^{(x-x_{\min}-1)}a_1(x_{\min},t+x_{\min}-x)\end{aligned} \tag{34a}$$

$$\begin{aligned}a_2(x,t)=&\sum_{\nu=0}^{(x_{\max}-x-1)}\Big[(-1)^{\nu}\Psi_2(x+1+\nu)\Phi_x(t-\nu)\Big]\\&-(-1)^{(x_{\max}-x-1)}a_2(x_{\max},t+x-x_{\max}).\end{aligned} \tag{34b}$$

The remaining amplitudes a_{3-8} can be calculated in an analogous way according to the mapping given by (13) and (14).

IV. Numerical Examples

In a numerical example, the spurious-mode-free excitation of a coplanar waveguide and of a triplate waveguide are compared to the traditional excitation scheme. For the extraction of a field template, we apply a Gaussian function $f(z=0,t)$ to the test section and we extract a template at the distance $z=-z_v$. The processing of the wave amplitude in the template according to (19) yields time functions Φ_z, which are depicted in Fig. 7. These functions describe the modifications made to the wave amplitudes for the rejection of spurious modes. The time functions representing the wave amplitudes a_9 and a_{11}, which are associated with the positive direction of propagation, hurry ahead of the Gaussian pulse, whereas

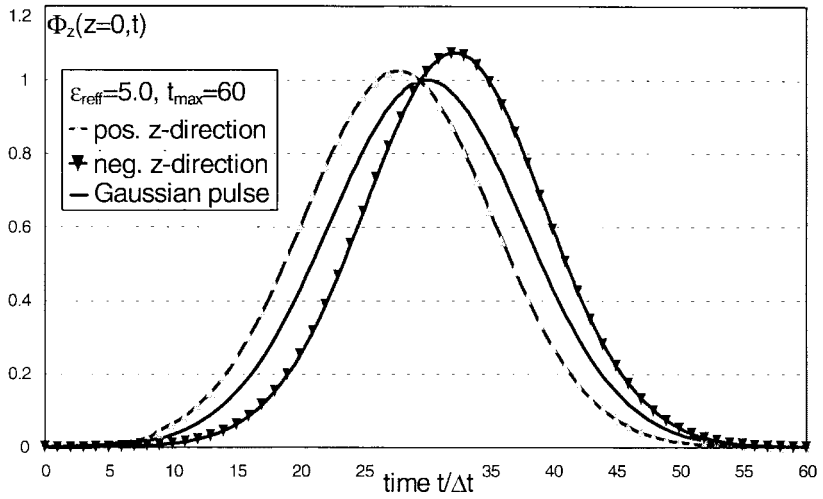

Fig. 7. Time histories Φ_z of the excitation of wave amplitudes in propagation direction with Gaussian shape and suppressed spurious mode.

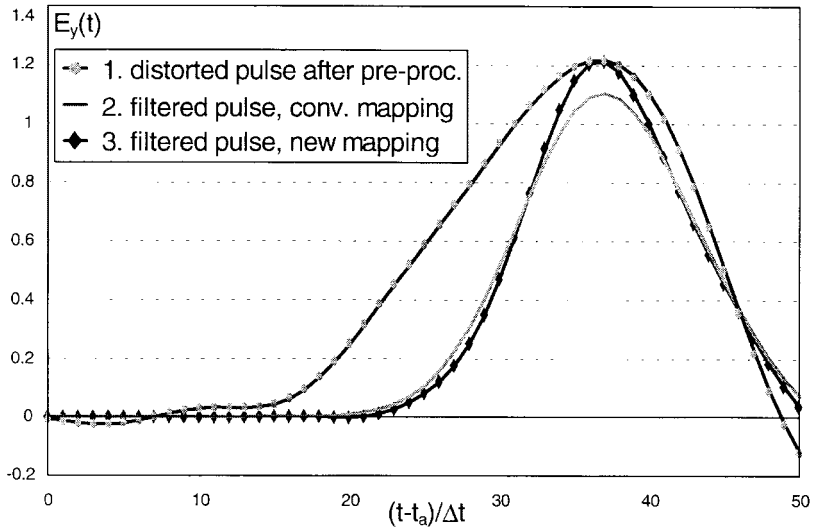

Fig. 8. Impulse responses to Gaussian excitation for different methods in the gate of a coplanar structure.

the functions representing the wave amplitudes a_{10} and a_{12}, associated with negative direction of propagation, lag behind the pulse. The shapes and amplitudes of these functions were mutually changed as well. For the extraction of the test section, we apply a Gaussian pulse with time window $t_{\max} = 60\ \Delta t$ and period $t_o = 13.3\ \Delta t$. We verify the method by the simulation of a coplanar waveguide (CPW) and a triplate waveguide section. The structures were discretized both in a coarse mesh 14×7 cells in cross section, emphasizing the occurrence of spurious modes in the conventional excitation. The temporal-field distribution generated from the excitation template is injected into the input section of the waveguide utilizing our mapping of the field amplitudes $a_1 - a_{18}$. In Figs. 8 and 9, three methods are compared: Signal one shows the impulse response to a Gaussian excitation after passing a coplanar waveguide section. Due to dispersion effects [3], [4], [9], [10] in the waveguides and because of the additional dispersion introduced by the TLM mesh, the pulse became distorted and spurious modes are visible in the signal. They are generated by an nonphysical excitation of the waveguide sections and gain more influence at the discontinuities of the circuits. These spurious modes are filtered by using the temporal maximum of the field distribution of signal one as a field template with a Gaussian time history to approach the physical-field excitation. With the use of the conventional mapping of the field distribution on the wave amplitudes of the TLM algorithm, new spurious modes are generated. With that, some energy of the physical pulse is lost for the excitation of new spurious modes. This loss can be seen in the lower amplitude of signal two. Utilizing our new approach for the mapping between field components and wave amplitudes the results are in good agreement to the amplitude of the field distribution in the excitation. This improved pulse response is shown as signal three. The energy of the excitation is now used only for the excitation of the physical pulse. In the case of the triplate structure, a resting deviation in the maximum can be seen. It comes from resting little shares of other physical modes which have been conserved during the preprocessing step. This effect can be further reduced by elongating the test section of the preprocessing.

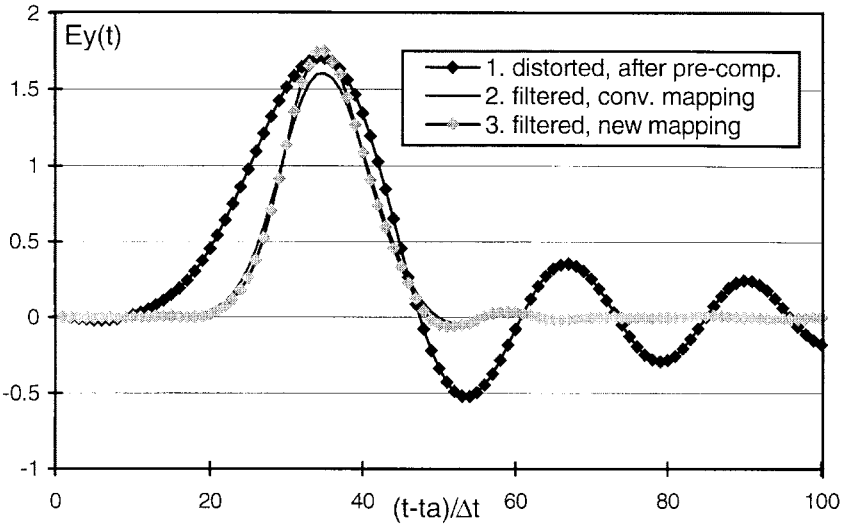

Fig. 9. Impulse responses to Gaussian excitation for different methods in the gate of a triplate structure.

V. Conclusion

A method for the suppression of spurious modes in the excitation of TLM meshes is presented. The method is applicable in general to the simulation of planar structures with dielectric, anisotropic, and lossy media. A separate analytical description of the excitation of the spurious modes and the physical modes is made in the $\boldsymbol{k}$–ω space. A special mapping of the field excitation onto the wave amplitudes of the TLM algorithm prevents the emanation of the spurious modes completely. The application of the mapping in the $\boldsymbol{k}$–ω space is done for waveguides with low computational effort and is demonstrated by way of an example. For planar structures with spatial discontinuities, we use precomputed field templates at the input area of the 3-D structures. Because of the appearance of field singularities, the mapping in these structures is mainly done in the space domain based on the quasi-TEM propagation of the guided waves to keep the computational effort low. By using this new method, the appearance of spurious modes in the excitation is suppressed by very low expenditure of calculation time. The feasibility of the approach is demonstrated by way of an coplanar waveguide and a triplate waveguide, which are fed by a Gaussian pulse at one port. The results are compared with those obtained from simulations using a conventional excitation scheme and they show a significant suppression of spurious modes with the energy conservation also being preserved.

References

[1] P. B. Johns, "A symmetrical condensed node for the TLM method," *IEEE Trans. Microwave Theory Tech.*, vol. MTT-35, pp. 370–377, Apr. 1987.

[2] P. Naylor and R. A. Desai, "New three dimensional symmetrical condensed lossy node for solution of electromagnetic wave problems by TLM," *Electron. Lett.*, vol. 26, pp. 492–495, Mar. 1990.

[3] S. Lindenmeier, B. Isele, R. Weigel, and P. Russer, "Improved initial conditions for the symmetrical condensed TLM-node with respect to physical propagation characteristics," in *Progress Electromagnetics Res. Symp. PIERS*, Nordwijk, The Netherlands, July 1995 (CD-ROM, 4 pp.).

[4] ———, "A fast spatial domain method for the suppression of excitation-induced spurious modes in SCN-TLM," in *IEEE MTT-S Dig.*, vol. 1. San Francisco, CA, June 1996, pp. 351–354.

[5] J. S. Nielsen, "Spurious modes of the TLM condensed node formulation," *IEEE Microwave Guided Wave Lett.*, vol. 1, pp. 201–203, Aug. 1991.

[6] J. S. Nielsen and W. J. R. Hoefer, "Generalized dispersion analysis and spurious modes of the 2-D and 3-D TLM formulations," *IEEE Trans. Microwave Theory Tech.*, vol. 11, pp. 1375–1384, Aug. 1993.

[7] I. Wolff, "Finite difference time-domain simulation of electromagnetic fields and microwave circuits," *Int. J. Numerical Modeling*, vol. 5, pp. 163–182, 1992.

[8] C. J. Railton and J. P. McGeehan, "The use of mode templates to improve the accuracy of the finite difference time domain method," in *Proc. 21st EuMC*, Stuttgart, Germany, Sept. 1991, pp. 1278–1283.

[9] J. A. Morente, G. Gimenez, J. A. Porti, and M. Khalladi, "Dispersion analysis for a TLM mesh of symmetrical condensed nodes with stubs," *IEEE Trans. Microwave Theory Tech.*, vol. 43, pp. 452–456, Feb. 1995.

[10] P. Berini and K. Wu, "Comprehensive study of numerical anisotropy and dispersion in 3D-TLM meshes," *IEEE Trans. Microwave Theory Tech.*, vol. 43, pp. 1173–1181, May. 1995.

Stefan Lindenmeier (M'97) was born in Munich, Germany, in 1967. He received the Dipl.-Ing. and the Dr.-Ing. degrees in electrical engineering from the Technical University of Munich, Munich, Germany, in 1994 and 1996, respectively.

From 1994 to 1996, he was with the Computer-Aided Design Department, Ferdinand Braun Institut Berlin, Germany, where he was working on numerical techniques for the field-theoretical analysis of microwave circuits. In 1996, he joined the Lehrstuhl für Hochfrequenztechnik, Technische Universität München, Munich, Germany, as an Assistant Professor. His current research interests are the development and application of CAD tools for the analysis of EMC problems, MMIC, and antenna design.

Bertram Isele was born in Tiengen, Germany, in 1965. He received the Dipl.-Ing. degree from the Technical University of Munich, Munich, Germany, in 1990, and is currently working toward the Ph.D. degree.

Since 1991, he has been with the Lehrstuhl für Hochfrequenztechnik at the Technische Universität München, Munich, Germany. His current research interests are computational techniques for the field analysis of microwave circuits and signal-processing.

Robert Weigel (S'84–M'86–SM'95) was born in Ebermannstadt, Germany, in 1956. He received the Dr.-Ing. and Dr.-Ing.habil. degrees in electrical engineering from the Technical University of Munich, Munich, Germany, in 1989 and 1992, respectively.

Since 1982, he has been with the Technical University of Munich, working as a Research Assistant (1982–1988), Senior Research Engineer (1988–1994), and Professor (1994–1996). In winter 1994/1995, he was a Guest Professor at the Technical University of Vienna, Vienna, Austria. Since 1996, he has been Head of the Institute for Communication and Information Engineering, University of Linz, Linz, Austria. He has been engaged in research and development on microwave theory and techniques, integrated optics, high-temperature superconductivity, surface acoustic wave (SAW) technology, and digital and microwave communication systems. He has published over 120 papers and has given more than 90 international presentations.

Dr. Weigel is a senior member of MTT-S Ultrasonics, Ferroelectrics, and Frequency Control societies, and a member of the Institute for Systems and Components of The Electromagnetics Academy, the Informationstechnische Gesellschaft (ITG) in the Verband Deutscher Elektrotechniker (VDE), and the Society of Photo Optical Instrumentation Engineers (SPIE). His review work includes European research projects and international journals. He was co-recipient of the MIOP award in 1993.

Peter Russer (SM'81–F'94) was born in Vienna, Austria, in 1943. He received the Dipl. Ing. and Dr. Techn. degrees in electrical engineering from the Technische Universität, Vienna, Austria, in 1967 and 1971, respectively.

From 1968 to 1971, he was an Assistant Professor at the Technische Universität. In 1971, he joined the Research Institute of AEG-Telefunken, Ulm, Germany, where he worked on fiber-optic communication, broad-band solid-state electronic circuits, statistical noise analysis of microwave circuits, laser modulation, and fiber-optic gyroscopes. Since 1981, he has been Chair of Hochfrequenztechnik at the Technische Universität München, Munich, Germany. From 1992 to 1995, he also has been the Director of the Ferdinand-Braun-Institut für Höchstfrequenztechnik, Berlin, Germany. He has authored over 200 scientific papers. His current research interests are integrated microwave and millimeter-wave circuits, electromagnetic fields, statistical noise analysis of microwave circuits, and methods for computer-aided design of microwave circuits.

Dr. Russer is a member of the German Informationstechnische Gesellschaft, and the Austrian and German Physical societies. He was co-recipient of the NTG Award in 1979.